International Journal of Thermal Sciences 49 (2010) 118–130

Contents lists available at ScienceDirect

International Journal of Thermal Sciences

journal homepage: www.elsevier.com/locate/ijts

Artificial neural network models for predicting electrical resistivity of soils from their thermal resistivity

Yusuf Erzin [a], B. Hanumantha Rao [b], A. Patel [b], S.D. Gumaste [b], D.N. Singh [b,*]

[a] Department of Civil Engineering, Celal Bayar University, 45140 Manisa, Turkey
[b] Department of Civil Engineering, Indian Institute of Technology Bombay, Mumbai 400076, India

ARTICLE INFO

Article history:
Received 12 February 2008
Received in revised form
2 April 2009
Accepted 24 June 2009
Available online 21 July 2009

Keywords:
Artificial neural networks
Soils
Electrical resistivity
Thermal resistivity
Generalized relationships

ABSTRACT

The knowledge of soil electrical and thermal resistivities is essential for several engineering projects such as laying of high voltage buried power cables, nuclear waste disposal, design of fluidized thermal beds, ground modification techniques etc. This necessitates precise determination of these resistivities, and relationship between them, which mainly depend on the soil type, its origin, compaction density and saturation. Such a relationship would also be helpful for determining one of these resistivities, if the other one is known. With this in view, efforts were made to develop artificial neural network (ANN) models that can be employed for estimating the soil electrical resistivity based on its soil thermal resistivity and the degree of saturation. To achieve this, measurements of electrical and thermal resistivities were carried out on different types soils compacted at different densities and moisture contents. These models were validated by comparing the predicted results vis-à-vis those obtained from experiments. The efficiency of these ANN models in predicting the soil electrical resistivity has been demonstrated, if its thermal resistivity is known. These ANN models are found to yield better results as compared to the generalized relationships proposed by the earlier researchers.

1. Introduction

The soil electrical resistivity, R_E, is a measure of the resistance offered by the soil against passage of current through it. The knowledge of R_E has been used to predict various soil parameters, phenomenon and mechanisms occurring in soils, such as for obtaining the soil water content [1], degree of compaction [2] and saturation [3], estimating liquefaction potential of the soil [4], detecting and locating geomembrane failures [5], to estimate corrosive effects of soil on buried steel [6], for designing earthing resistance of the grounding systems [7], to study the electro-osmosis phenomenon in soils [8], investigating the effects of soil freezing [9] and for estimating the soil salinity for agricultural activities [10].

These studies highlight that determination of R_E, depends on several parameters such as frequency of the current used, geometry and type of the electrodes used etc., and is a cumbersome process [11]. While, soil thermal resistivity, R_T, can be determined easily and rapidly by employing the transient heat method [12–15]. In addition, both R_E and R_T are strongly influenced by soil type, its origin and the degree of saturation. Based on the transient heat method generalized relationships have been developed, which can be utilized for determining R_T [15,16].

Hence, determination of R_E of the soil by relating it to its R_T would be of great help to professionals. Singh et al. [17] have proposed the following generalized relationship between R_E and R_T as follows:

$$\log(R_E) = C_R \log(R_T) \tag{1}$$

where C_R is a constant and its values can be obtained from Eq. (2):

$$C_R = 1.34 + 0.0085 \times F \tag{2}$$

where F is the percentage sum of the gravel and sand size fractions in the soil.

However, it must be noted that Eq. (2) does not take into account the saturation, S_r, of the soil, which influences both R_E and R_T [18], quite substantially. To overcome this limitation, Sreedeep et al. [18] proposed Eq. (3).

$$C_R = X + Y \cdot e^{(-S_r \times Z)} \tag{3}$$

where X, Y and Z are constant parameters, which mainly depend on the type of the soil, as depicted in Equations (4)–(6), respectively.

* Corresponding author. Tel.: +91 22 25767340; fax: +91 22 25767302.
E-mail addresses: yusuf.erzin@bayar.edu.tr (Y. Erzin), hanuma_bendadi@iitb.ac.in (B.H. Rao), apatel@iitb.ac.in (A. Patel), p7suchitdg@civil.iitb.ac.in (S.D. Gumaste), dns@civil.iitb.ac.in (D.N. Singh).

1290-0729/$ – see front matter © 2009 Elsevier Masson SAS. All rights reserved.
doi:10.1016/j.ijthermalsci.2009.06.008

Nomenclature

γ_d	dry-unit weight of the soil (g/cc)
μ	momentum factor
ρ	resistance per unit length (Ω/cm)
C_R	constant
F	percentage sum of the gravel and sand size fractions (%)
G	specific gravity
i	current (Amp)
I	number of input parameters
Learngdm	gradient descent with momentum weight/bias learning function
MAE	mean absolute error
N_{h1}	lnumber of neurons in the hidden layer
Q	heat input per unit length
R_E	electrical resistivity (Ω m)
RMSE	root mean square error
R_T	thermal resistivity (°C.m/W)
S_r	degree of saturation (%)
Trainlm	Levenberg-Marquardt training algorithm
Trainscg	Scaled Conjugate Gradient training algorithm
VAF	variance account for
var	variance
w	moisture content (%)
x	actual value
X, Y, & Z	constant parameters
x_{max}	maximum value
x_{min}	minimum value
x_{norm}	normalized value
y	measured value
$\hat{y}$	predicted value

$$X = [1.1 + 0.01 \times F] \tag{4}$$

$$Y = [0.9 - 0.01 \times F] \tag{5}$$

$$Z = \left[0.02 + 0.0006 \times e^{(F/25)}\right] \tag{6}$$

Though, the utility and efficiency of these relationships was demonstrated by Sreedeep et al. [18], these relationships are derived based on simple interpolation and extrapolation of experimental results obtained by testing different types of locally available soils compacted at different densities and moisture content. Hence, in order to generate much confidence in using these relationships, better computational algorithms (viz., artificial neural networks) that are capable of incorporating the interdependence of several parameters must be employed.

Artificial neural networks (ANNs) offer an interesting approach for modeling soil behavior [19–21]. ANN is an oversimplified simulation of the human brain [21] and is accepted as a reliable data-modeling tool to capture and represent complex relationships between inputs and outputs [22]. Recently, ANNs have been effectively applied to model the behavior of the soil such as liquefaction of soils [23], soil classification [24], compaction of soils [25], determination of pile capacity [26,27], settlement analysis [28], thermal properties of soils [29] and stress-strain modeling [21,30].

With this in view, efforts were made to develop ANN models that can be employed for predicting R_E by employing different soil properties such as R_T, S_r and F. To show the efficiency of these models, results predicted from them were compared vis-à-vis those obtained from Equations (1)–(3). In addition, the performance indices such as coefficient of determination, root mean square error, mean absolute error, and variance were used to assess the performance of the ANN models.

2. Artificial Neural Networks

Artificial neural networks (ANNs) are computational model, which is based on the information processing system of the human brain [21]. The current interest in ANNs is largely due to their ability to mimic natural intelligence in its learning from experience [31–35]. A typical structure of ANNs is composed of a number of interconnected processing elements (PEs), commonly referred to as neurons. The neurons are logically arranged in layers: an input layer, an output layer and one or more hidden layers. The neurons interact with each other via weighted connections. Each neuron is connected to all the neurons in the next layer. The input layer is the means by which data are presented to the network. The output layer holds the response of the network to the input. The hidden layers enable these networks to represent and compute complicated associations between inputs and outputs. This ANN architecture is commonly referred to as a fully interconnected feed-forward multi-layer perceptron (MLP). In addition, there is also a bias, which is only connected to neurons in the hidden and output layers, with modifiable weighted connections.

Currently, there is no analytical way of defining the network structure as a function of the complexity of the problem. The structure must be manually selected using a trial-and-error process. ANNs with one or two hidden layers and adequate number of hidden neurons are found to be quite useful for most problems [36,37]. The number of neurons in the hidden layers depends on the nature of the problem. There are various methods to determine the number of neurons in the hidden layer [38–41]. However, these methods present general guidelines only for selection of an adequate number of neurons.

The back-propagation learning algorithm is the most popular and extensively used neural network algorithm [42,43]. The back-propagation neural network has been applied with great success to model many phenomena in the field of geotechnical and geo-environmental engineering [44–46]. The back-propagation learning algorithm basically involves two phases: the feed-forward pass and backward pass process. In the forward phase, the processing of information is propagated from the input layer to the output layer. In the backward phase, the difference between obtained network output value from feed-forward process and desired output is propagated backwards in order to modify the weightings and bias values. The training of the network is achieved by adjusting the weights and is carried out through a large number of training sets and training cycles. The goal of the training procedure is to find the optimal set of weights which would produce the right output for any input in the ideal case [22]. Training the weights of the network is iteratively adjusted to capture the relationships between the input and output patterns.

The performance of the overall ANN model can be assessed by several criteria [21,47–49]. These criteria include coefficient of determination R^2, mean squared error, mean absolute error, minimal absolute error, and maximum absolute error. A well-trained model should result in an R^2 value close to 1 and small values of error terms.

In this study, prediction of electrical resistivity, R_E, of the soil has been modeled using the ANN and multiple regression

Table 1
Details of the onshore samples.

Sample	G	F (%)	w (%)	γ_d (g/cc)	S_r (%)	R_T (°C m/W)	R_E (Ω m)	$C_{R(EXPT.)}$	C_R(Eq. (3))	C_R(Eq. (2))	USCS
A	2.67	100	1.06	4.64	8.2	2.62	526.32	1.95	2.04	2.19	SP
			1.45	4.78	15.2	1.47	232.56	2.02	2.06	2.19	
			1.62	4.36	18.0	1.21	169.49	2.03	2.06	2.19	
			1.72	4.42	21.6	1.04	156.25	2.08	2.07	2.19	
			1.36	13.11	36.5	1.08	126.58	2.02	2.09	2.19	
			1.57	12.57	48.2	0.81	92.59	2.08	2.09	2.19	
			1.71	12.60	60.5	0.66	80	2.15	2.1	2.19	
			1.81	12.16	68.6	0.58	71.43	2.19	2.1	2.19	
B	2.58	55	1.29	9.71	25.2	2.4	18.38	1.37	1.83	1.81	SC
			1.47	9.43	32.2	1.91	11	1.33	1.8	1.81	
			1.62	9.94	43.2	1.46	7.54	1.33	1.77	1.81	
			1.77	9.40	53.2	1.24	5.86	1.32	1.74	1.81	
			1.54	15.57	59.4	1.15	1.66	1.08	1.73	1.81	
			1.68	15.08	72.1	0.96	2.22	1.18	1.71	1.81	
			1.78	14.64	83.8	0.85	4.28	1.36	1.69	1.81	
C	2.64	76	1.56	9.67	36.8	1.16	82.64	1.9	1.9	1.99	SM
			1.90	9.60	64.8	0.72	49.26	1.99	1.88	1.99	
			1.99	8.84	72.0	0.67	42.55	1.98	1.87	1.99	
			2.13	8.61	94.2	0.56	38.02	2.04	1.87	1.99	
			1.84	12.39	75.5	0.66	29.07	1.9	1.87	1.99	
			1.94	12.54	91.2	0.57	21.46	1.9	1.87	1.99	
			2.04	12.39	110.6	0.49	18.87	1.93	1.86	1.99	
			2.05	12.06	111.2	0.5	18.25	1.92	1.86	1.99	
D	2.7	12	1.29	10.33	25.4	3.18	64.1	1.52	1.68	1.44	ML
			1.52	10.30	36.0	2.29	29.85	1.47	1.59	1.44	
			1.64	10.24	42.9	1.94	23.15	1.47	1.54	1.44	
			1.72	9.75	46.3	1.82	20.79	1.47	1.52	1.44	
			1.25	15.99	37.2	2.33	46.3	1.55	1.58	1.44	
			1.49	15.33	51.1	1.7	21.41	1.49	1.49	1.44	
			1.63	15.16	62.6	1.4	15.58	1.49	1.43	1.44	
			1.78	14.45	75.8	1.17	12.25	1.49	1.38	1.44	
E	2.56	60	1.15	9.83	20.5	2.6	105.26	1.67	1.87	1.85	GC
			1.31	11.41	30.7	1.82	60.61	1.67	1.83	1.85	
			1.44	11.26	37.0	1.52	47.17	1.68	1.81	1.85	
			1.60	10.30	44.4	1.31	32.68	1.66	1.79	1.85	
			1.32	15.37	41.8	1.46	42.55	1.68	1.8	1.85	
			1.47	16.09	55.9	1.15	33.44	1.71	1.77	1.85	
			1.76	12.18	68.3	0.91	25.45	1.74	1.75	1.85	
			1.85	13.62	90.8	0.74	21.01	1.78	1.73	1.85	
F	2.64	35	1.27	9.26	22.7	3.13	14.73	1.27	1.78	1.64	CL
			1.46	9.33	30.6	2.36	8.85	1.24	1.73	1.64	
			1.56	9.12	34.7	2.1	7.55	1.24	1.7	1.64	
			1.66	8.89	39.9	1.88	6.08	1.22	1.67	1.64	
			1.36	17.07	47.8	1.65	2.68	1.09	1.64	1.64	
			1.53	14.93	54.4	1.41	2.2	1.09	1.61	1.64	
			1.70	15.05	72.3	1.1	1.73	1.1	1.56	1.64	
G	2.6	20	1.23	11.30	26.4	2.99	36.23	1.44	1.7	1.51	CH
			1.44	11.61	37.6	2.16	19.01	1.4	1.61	1.51	
			1.51	11.60	42.1	1.96	14.22	1.38	1.59	1.51	
			1.63	10.80	47.5	1.76	11.29	1.36	1.55	1.51	
			1.35	19.58	54.7	1.69	5.17	1.22	1.52	1.51	
			1.45	18.70	61.2	1.5	5.42	1.26	1.49	1.51	
			1.60	18.49	77.4	1.22	6.48	1.35	1.43	1.51	
H	2.64	24	1.27	10.56	25.7	3.13	28.74	1.39	1.72	1.54	CH
			1.49	8.80	30.1	2.84	41.32	1.47	1.69	1.54	
			1.40	11.20	33.5	2.44	11.78	1.29	1.66	1.54	
			1.40	13.42	40.1	2.07	6.49	1.21	1.62	1.54	
			1.29	17.54	44.5	1.99	4.33	1.15	1.59	1.54	
I	2.66	23	1.50	9.99	34.4	2.48	39.37	1.50	1.65	1.54	CH
			1.43	12.66	39.1	2.15	11.11	1.31	1.62	1.54	
			1.36	13.71	38.3	2.22	5.75	1.18	1.62	1.54	
			1.33	16.13	43.2	2.04	3.88	1.12	1.59	1.54	
J	2.65	24	1.51	9.4	32.9	2.55	38.17	1.49	1.66	1.54	CH
			1.50	10.7	37.0	2.23	16.21	1.37	1.64	1.54	
			1.41	12.57	38.0	2.17	5.49	1.17	1.63	1.54	
			1.25	18.96	45.0	2.02	3.64	1.11	1.59	1.54	
K	2.56	23	1.47	9.2	32.0	2.90	34.60	1.44	1.67	1.54	CH
			1.52	10.37	38.9	2.33	12.17	1.30	1.62	1.54	
			1.34	19.04	53.9	1.81	2.29	1.04	1.54	1.54	
L	2.65	27	1.44	11.38	35.7	2.25	17.89	1.38	1.66	1.57	CH
			1.42	12.75	39.0	2.09	10.53	1.30	1.64	1.57	
			1.51	8.86	30.9	2.72	28.90	1.42	1.69	1.57	
			1.29	20.33	51.0	1.80	2.85	1.09	1.58	1.57	

Table 1 (*continued*)

Sample	G	F (%)	w (%)	γ_d (g/cc)	S_r (%)	R_T (°C m/W)	R_E (Ω m)	$C_{R(EXPT.)}$	C_R(Eq. (3))	C_R(Eq. (2))	USCS
M	2.62	22.5	1.47	9.87	32.8	2.60	33.22	1.46	1.66	1.53	CH
			1.47	11.37	38.2	2.23	14.39	1.34	1.62	1.53	
			1.35	13.52	37.5	2.26	7.09	1.21	1.63	1.53	
			1.41	12.56	38.5	2.21	6.45	1.20	1.62	1.53	
			1.34	19.4	53.2	1.77	4.63	1.19	1.54	1.53	
N	2.56	21	1.37	9.88	28.9	3.10	38.02	1.44	1.68	1.52	CH
			1.37	11.62	34.3	2.59	11.99	1.28	1.64	1.52	
			1.40	12.91	39.9	2.25	6.14	1.19	1.60	1.52	
			1.31	17.19	46.4	2.05	2.97	1.07	1.57	1.52	
			1.34	22.84	63.7	1.64	2.09	1.05	1.49	1.52	
O	2.64	27.5	1.40	8.9	26.7	3.15	62.89	1.52	1.72	1.57	CH
			1.44	12.8	40.3	2.01	8.06	1.26	1.63	1.57	
			1.43	14.62	45.7	1.83	5.18	1.20	1.61	1.57	
			1.33	14.15	38.0	2.16	4.74	1.15	1.65	1.57	
			1.20	21.88	48.0	1.95	3.07	1.09	1.59	1.57	
P	2.61	36	1.51	8.27	29.9	2.68	38.02	1.47	1.74	1.65	CI
			1.53	7.84	29.0	2.83	17.06	1.32	1.74	1.65	
			1.35	16.45	45.9	1.74	5.08	1.21	1.65	1.65	
			1.43	22	69.2	1.30	2.06	1.09	1.57	1.65	
Q	2.67	25	1.49	7.95	26.9	3.18	33.00	1.41	1.71	1.55	CI
			1.52	8.94	31.7	2.57	14.29	1.31	1.68	1.55	
			1.38	13.21	37.6	2.11	9.17	1.27	1.64	1.55	
			1.49	19.12	64.9	1.39	4.78	1.25	1.51	1.55	
			1.28	24.6	60.1	1.63	1.86	1.03	1.53	1.55	
R	2.57	35	1.32	16.4	44.7	1.86	6.17	1.23	1.65	1.64	CH
			1.31	19.97	53.3	1.67	4.76	1.21	1.62	1.64	
S	2.66	23.5	1.39	11.08	32.1	2.54	16.81	1.34	1.67	1.54	CH
			1.39	18.71	54.5	1.67	4.93	1.21	1.54	1.54	
			1.18	28.75	61.0	1.78	2.38	1.06	1.51	1.54	
T	2.61	35.5	1.49	9.4	32.6	2.36	17.48	1.37	1.72	1.64	CH
			1.41	17.95	54.8	1.52	2.85	1.13	1.61	1.64	
			1.28	22.2	55.4	1.62	1.82	1.02	1.61	1.64	

analysis (MRA). In ANN models, network training was accomplished with the neural network toolbox written in Matlab environment [50]. While, the Levenberg-Marquardt [50] and the Scaled Conjugate [51] learning algorithms were used in the training stage. Details of the experimental investigations, which have yielded the data used in both models, are presented in the following section.

3. Experimental investigations

Undisturbed soil samples from various onshore and offshore locations in India, where major infrastructure development is taking place, were collected. For establishing particle-size distribution characteristics of these samples, dry-sieving, and whenever required hydrometer analysis, was conducted [52]. The specific gravity G of these materials was determined by using an Ultra-pycnometer (Quantachrome®, USA), which employs Helium gas [53]. For the sake of generality, six tests were conducted on each soil sample and the average value was considered as the representative G, as listed in Tables 1 and 2 for the onshore and offshore samples, respectively. The sulphite and chloride contents of onshore samples are found to be 5–10 ppm, and 25–50 ppm, respectively. However, for the offshore samples the sulphite and chloride contents are quite high (5–10 ppm, and 500–1000 ppm), respectively. These samples were also tested for R_E and R_T, respectively, as described in the following, and the results are presented in Table 1 and Table 2, respectively.

Table 2
Details of the offshore samples.

G	F (%)	w (%)	γ_d (g/cc)	S_r (%)	R_T (°C m/W)	R_E (Ω m)	USCS
2.49	1	63.45	0.96	99.6	2.05	1.28	CH
2.52	2	63.57	0.97	100.0	1.80	0.61	CH
2.53	1	53.88	0.97	84.9	1.99	0.74	MH
2.61	1	75.52	0.88	99.9	2.20	0.93	CH
2.48	1	64.89	0.95	99.8	2.06	0.96	CH
2.48	1	64.80	0.94	97.6	2.07	0.78	CH
2.51	1	58.43	1.02	99.9	1.93	0.97	CH
2.45	5	71.43	0.89	99.9	2.07	0.97	CH
2.5	1	57.12	1.03	99.9	1.83	0.93	CH
2.49	1	59.26	1.01	99.9	1.92	0.92	CH
2.53	1	54.91	1.06	100.0	1.80	0.84	CH
2.51	1	61.65	0.98	99.9	2.00	0.76	CH
2.42	5	57.59	1.01	100.0	1.92	0.70	CH
2.52	3	62.59	0.98	100.0	1.96	0.61	CH
2.48	1	56.33	1.03	99.9	1.84	0.75	CH
2.48	0	76.05	0.86	100.0	2.24	0.60	CH
2.49	5	52.75	1.07	99.6	1.89	0.67	CH
2.46	0	59.03	1.00	100.0	2.03	1.42	CH

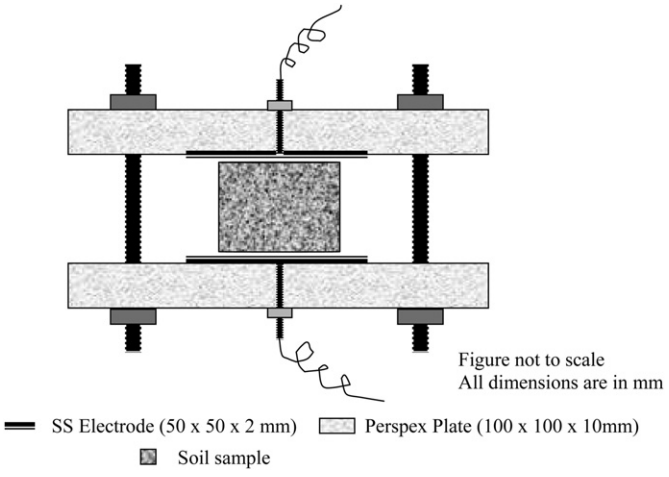

Fig. 1. The setup used for determining electrical resistivity of the soil sample.

Table 3
R_E and R_T of the soils used by Sreedeep et al. [18] and Abu-Hassanein [11].

Soil	G	F	w (%)	γ_d (g/cc)	S_r (%)	R_T (°C.m/W)	R_E (Ω.m)	$C_{R(EXPT.)}$	C_R(Eq. (3))	C_R(Eq. (2))
1	2.65	0	9.8	0.89	13.1	39.22	329.42	1.26	1.79	1.34
			16.1	1.03	27.6	19.81	111.96	1.23	1.61	1.34
			18.1	1.0	29.6	20.68	119.79	1.23	1.59	1.34
			16.7	1.06	30.0	18.83	106.39	1.23	1.59	1.34
			17	1.12	33.7	18.12	86.58	1.21	1.55	1.34
			21.2	1.17	45.4	13.75	62.9	1.21	1.45	1.34
			25.9	1.13	52.1	56.04	13.89	1.19	1.41	1.34
			27.7	1.17	59.1	47.19	12.62	1.18	1.37	1.34
			29.8	1.26	73.3	25.39	8.52	1.16	1.30	1.34
			30.7	1.29	79	17.91	7.31	1.14	1.28	1.34
			37.1	1.25	89.8	26.96	8.38	1.17	1.24	1.34
			38.7	1.24	92.1	55.14	12.45	1.21	1.23	1.34
2	2.75	24	–	–	41	10.60	44.77	1.21	1.61	1.54
			–	–	46	10.17	43.83	1.21	1.58	1.54
			–	–	54	8.00	27.87	1.19	1.55	1.54
			–	–	63	7.30	25.53	1.19	1.51	1.54
			–	–	64	6.42	18.19	1.16	1.51	1.54
			–	–	78	6.70	22.63	1.19	1.46	1.54
			–	–	79	6.49	23.17	1.20	1.46	1.54
			–	–	87	5.66	16.58	1.17	1.44	1.54
			–	–	90	5.42	15.21	1.16	1.43	1.54
			–	–	90	5.16	13.36	1.15	1.43	1.54
			–	–	91	5.38	15.02	1.16	1.43	1.54
			–	–	93	5.16	13.83	1.16	1.43	1.54
			–	–	94	5.55	17.21	1.18	1.43	1.54
			–	–	96	5.24	14.62	1.16	1.42	1.54
			–	–	97	5.25	15.15	1.17	1.42	1.54
3	2.80	6	–	–	38	10.02	28.94	1.15	1.54	1.39
			–	–	39	8.87	22.67	1.14	1.53	1.39
			–	–	47	6.27	11.71	1.10	1.48	1.39
			–	–	53	5.28	8.99	1.08	1.44	1.39
			–	–	60	5.23	9.17	1.09	1.40	1.39
			–	–	66	5.32	10.73	1.11	1.37	1.39
			–	–	71	4.50	7.51	1.08	1.35	1.39
			–	–	71	4.51	7.64	1.09	1.35	1.39
			–	–	87	3.98	6.36	1.08	1.30	1.39
			–	–	87	3.51	5.25	1.07	1.30	1.39
			–	–	92	3.71	5.8	1.08	1.28	1.39
			–	–	95	3.45	5.25	1.07	1.28	1.39
			–	–	97	3.26	4.94	1.07	1.27	1.39
			–	–	99	3.13	4.45	1.06	1.27	1.39
4	2.69	47	–	–	41	13.18	82.28	1.26	1.73	1.74
			–	–	46	11.69	66.99	1.25	1.71	1.74
			–	–	55	10.05	52.93	1.24	1.69	1.74
			–	–	59	9.85	47.72	1.23	1.67	1.74
			–	–	71	8.16	34.03	1.21	1.65	1.74
			–	–	75	7.67	30.64	1.21	1.64	1.74
			–	–	78	7.89	31.5	1.21	1.64	1.74
			–	–	80	8.33	33.06	1.20	1.63	1.74
			–	–	89	7.28	29.22	1.21	1.62	1.74
			–	–	91	6.78	24.92	1.20	1.62	1.74
			–	–	92	7.58	31.27	1.21	1.62	1.74
			–	–	94	7.49	31.29	1.22	1.62	1.74
			–	–	95	7.54	30.41	1.21	1.61	1.74
			–	–	99	7.02	26.91	1.21	1.61	1.74
5	2.80	38	–	–	32	13.37	70.27	1.23	1.73	1.66
			–	–	37	11.53	53.81	1.22	1.70	1.66
			–	–	50	8.36	34.66	1.21	1.65	1.66
			–	–	56	9.49	46.91	1.23	1.63	1.66
			–	–	58	7.39	28.78	1.21	1.62	1.66
			–	–	67	10.43	53.81	1.24	1.59	1.66
			–	–	86	6.82	28.78	1.22	1.55	1.66
			–	–	87	5.91	21.99	1.21	1.55	1.66
			–	–	92	5.61	20.09	1.20	1.54	1.66
			–	–	93	5.63	20.56	1.20	1.54	1.66
			–	–	94	5.46	19.2	1.20	1.54	1.66
			–	–	95	5.47	18.9	1.20	1.54	1.66
			–	–	96	5.67	21.55	1.21	1.54	1.66
			–	–	100	5.96	24.42	1.22	1.89	1.66
6	2.70	6	–	–	34	8.16	16.65	1.11	1.57	1.39
			–	–	36	8.52	18.82	1.12	1.56	1.39
			–	–	43	6.67	12.72	1.10	1.50	1.39
			–	–	50	5.84	10.65	1.09	1.46	1.39
			–	–	54	5.25	9.23	1.09	1.43	1.39

Table 3 (*continued*)

Soil	G	F	w (%)	γ_d (g/cc)	S_r (%)	R_T (°C.m/W)	R_E (Ω.m)	$C_{R(EXPT.)}$	C_R(Eq. (3))	C_R(Eq. (2))
			–	–	62	4.83	8.26	1.09	1.39	1.39
			–	–	64	4.47	7.21	1.08	1.38	1.39
			–	–	72	4.47	7.54	1.09	1.35	1.39
			–	–	73	4.09	6.52	1.08	1.34	1.39
			–	–	82	3.90	6.11	1.08	1.31	1.39
			–	–	88	3.74	6.02	1.08	1.30	1.39
			–	–	90	3.69	5.99	1.08	1.29	1.39
			–	–	94	3.56	5.56	1.08	1.28	1.39
			–	–	96	3.31	4.97	1.07	1.27	1.39
7	2.80	6	–	–	58	8.69	28.56	1.18	1.41	1.39
			–	–	74	6.10	14.52	1.14	1.34	1.39
			–	–	90	5.18	9.85	1.10	1.29	1.39
			–	–	92	4.73	8.66	1.10	1.28	1.39
			–	–	95	4.94	9.97	1.11	1.28	1.39
8	2.78	19	–	–	42	6.48	13.67	1.12	1.58	1.50
			–	–	62	4.73	8.94	1.06	1.48	1.50
			–	–	89	4.06	7.95	1.07	1.40	1.50
			–	–	91	4.01	7.8	1.08	1.39	1.50
			–	–	92	4.20	8.37	1.09	1.39	1.50
9	2.68	48	–	–	36	11.29	54.57	1.22	1.76	1.75
			–	–	59	7.93	35.21	1.22	1.68	1.75
			–	–	86	7.37	41.88	1.26	1.63	1.75
			–	–	87	6.31	25.56	1.22	1.63	1.75
			–	–	100	5.74	22.86	1.22	1.62	1.75
10	2.68	36	–	–	41.6	18.60	377.82	1.40	1.67	1.65
			–	–	63	14.41	243.76	1.39	1.59	1.65
			–	–	91.1	12.05	168.45	1.37	1.53	1.65
			–	–	93.5	13.09	162.85	1.35	1.53	1.65
			–	–	93.7	12.19	141.43	1.34	1.53	1.65
11	2.67	46	–	–	24	16.73	90.71	1.24	1.75	1.73
			–	–	36	11.43	62.88	1.26	1.62	1.73
			–	–	82	7.25	40.67	1.22	1.62	1.73
			–	–	87	6.56	27.94	1.24	1.61	1.73
			–	–	90	6.69	31.23	1.13	1.59	1.44
12	2.90	12	–	–	36	8.27	19.65	1.09	1.53	1.44
			–	–	44	5.58	10.02	1.09	1.37	1.44
			–	–	80	3.81	6.5	1.10	1.36	1.44
			–	–	83	3.91	7.04	1.10	1.35	1.44
			–	–	86	3.87	7.02	1.24	1.75	1.73

–: Data not available.

3.1. Measurement of electrical resistivity

The test setup depicted in Fig. 1 was fabricated and employed for measuring R_E of the sample. This setup made of Perspex, consists of two 10 mm thick square plates of size 100 mm and on one face of these plates a stainless steel plate of size $50 \times 50 \times 2$ mm, which acts as an electrode, is fitted. These electrodes are mirror-finished and passivated in order to avoid electrode polarization and to minimize the interfacial effect during the resistivity measurements. The bolt and screw mechanism helps in fixing the sample of different thicknesses in between the electrodes. From the UDS tube, a sample of size 38 mm diameter and 30 mm thickness was extruded and its weight and dimensions were recorded. This helps in determining the total unit weight, γ_t, of the sample. Later, this sample was trimmed and a conducting paint (Silver oxide) was applied on the top and bottom faces of the sample, which act as two electrodes. This arrangement helps in application of a uniform voltage difference across the sample when it is inserted between the plate electrodes. R_E of the sample was measurement by using an impedance analyzer (SOLARTRON®-1260) and fixing the frequency of AC as 2 Hz. During the experimentation room temperature (25 ± 1°C) and the relative humidity (60 ± 1%) were maintained. Later, the sample was kept in the oven to determine its gravimetric water content, w, and hence the dry-unit weight, γ_d.

Table 4
Boundaries of the parameters used for the models developed.

Data type	Model parameters	Minimum value	Maximum value
Input	S_r (%)	8	111
	F (%)	0	100
	R_T (°C m/W)	0.5	39.2
Output	R_E (Ω m)	0.6	526.3

3.2. Measurement of thermal resistivity

A thermal probe, which operates on the principle of "Transient method" [12–18,54], was fabricated and used in this study. The probe consists of an insulated Nichrome heater wire of resistance, ρ(=0.19 Ω/cm), inserted in a copper tube of 140 mm length and 2.5 mm external diameter. A thermocouple is attached on the inner surface of the tube. The heat input per unit length, Q, is equal to $i^2.\rho$ (in W/cm), where, i is the current passing in the heater wire. The calibration of this probe was achieved by using a standard liquid glycerol with thermal resistivity R_T equal to 349 °C cm/W [13,14,54]. The R_T of the glycerol was found to be equal to 357 °C cm/W (for $i = 0.5$ Amp), which is only 2.4% higher than the standard value. A metal container (150 mm long and 100 mm diameter) was used to prepare the soil samples corresponding to a particular density and moisture content. A 2 mm diameter hole was drilled in the soil sample and the thermal probe was fitted tightly into it. The probe was allowed to achieve thermal equilibrium in the soil mass for about 2 min and then the power supply to the probe was switched

Table 5
The details of the optimal performance of the ANN-1 model.

ANN-1 model	Training function used	Epoch number	Performance indices				
			Data set	MAE (Ω m)	RMSE (Ω m)	VAF (%)	R^2
211	*Trainlm*	15	Training	21.15	40.31	62.93	0.629
			Validation	15.28	26.74	64.38	0.644
			Testing	13.68	20.46	75.63	0.757
	Trainscg	37	Training	20.87	40.63	62.36	0.625
			Validation	15.82	26.92	64.45	0.645
			Testing	14.31	20.61	75.99	0.760
221	*Trainlm*	19	Training	14.86	25.57	85.09	0.851
			Validation	12.42	22.38	74.85	0.752
			Testing	9.68	14.06	89.16	0.894
	Trainscg	30	Training	20.60	41.62	60.53	0.629
			Validation	14.99	29.90	55.05	0.565
			Testing	11.52	19.90	76.55	0.767
231	*Trainlm*	23	Training	12.61	16.84	93.56	0.936
			Validation	9.18	12.07	92.74	0.928
			Testing	8.13	11.00	92.69	0.928
	Trainscg	37	Training	19.09	37.76	67.47	0.675
			Validation	11.52	19.88	80.10	0.802
			Testing	8.62	13.74	88.55	0.893
241	*Trainlm*	35	Training	10.65	15.64	94.43	0.944
			Validation	8.66	11.68	93.38	0.937
			Testing	7.65	9.93	94.67	0.951
	Trainscg	36	Training	16.61	31.39	78.32	0.784
			Validation	11.02	20.08	80.30	0.820
			Testing	8.23	12.95	90.44	0.913
251	*Trainlm*	39	Training	**10.68**	**15.67**	**94.41**	**0.944**
			Validation	**8.08**	**11.93**	**93.04**	**0.936**
			Testing	**6.67**	**9.15**	**95.54**	**0.957**
	Trainscg	34	Training	17.07	38.72	66.18	0.663
			Validation	11.68	23.13	73.31	0.769
			Testing	8.30	13.70	88.84	0.891

on. The temperature of the probe was recorded as a function of time and was used to compute the thermal resistivity of the soil [14,54].

4. Development of ANN models

As mentioned earlier, the multiplier C_R used in the relationship Eq. (2) includes the type of the soil (i.e. its physical composition) only, while C_R in the relationship Eq. (3) includes both the type of soil and its saturation. Keeping this in view, two ANN models (ANN-1 and ANN-2) were developed for predicting R_E. The model ANN-1 takes into account the effect of soil type only (and hence has two input parameters, F and R_T). While, the model ANN-2 takes into consideration the effect of both soil type and its saturation (and hence has three input parameters, S_r, F and R_T). Both models have one output parameter R_E.

In addition to the data obtained by conducting experiments on the onshore and offshore samples (refer Tables 1 and 2), the data reported by Sreedeep et al. [18] and Abu-Hassanein [11] for different types of soils, with their resistivities listed in Table 3, were also used to develop these models. It can be noticed from Table 3 that w and γ_d for soils 2–12 are not available and as such S_r, which reflects the compaction state of the soil mass was used as an input parameter in ANN-2 model. The boundaries for input and output parameters of the models are listed in Table 4. The input-output data of both ANN models were scaled to lie between 0 and 1 by using Eq. (7).

$$x_{norm} = \frac{(x - x_{min})}{(x_{max} - x_{min})} \tag{7}$$

where x_{norm} is the normalized value, x is the actual value, x_{max} is the maximum value and x_{min} is the minimum value.

It is a common practice to divide the available data into two subsets; a training set, to construct the neural network model, and an independent validation set to estimate model performance in the deployed environment [55]. However, dividing the data into only two subsets may lead to model over fitting. Over fitting makes multi-layer perceptrons (MLPs) memorize training patterns in such a way that they cannot generalize well to new data [21]. As a result, cross validation technique [56] was used as the stopping criterion in this study. In this technique, the database is divided into three subsets: training, validation and testing. The training set is used to update networks' weights. One pass through the set of training patterns together with the associated updating of the weights is called a cycle or an epoch. During this process the error on the validation set is monitored. When the error on the validation set begins to increase, the training is stopped because it is considered to be the best point of generalization. Finally, testing data is fed into the networks to evaluate their performance. Therefore, a dataset of 236 (listed in Tables 1–3) was divided randomly into three subsets: training (56%), testing (24%), and validation (20%). Training dataset includes 132 soils (59 onshore soils, 11 offshore soils and 62 soils used by Sreedeep et al. [18] and Abu-Hassanein [11]). Testing dataset includes a dataset of 57 (25 onshore soils, 4 offshore soils and 28 soils used by Sreedeep et al. [18] and Abu-Hassanein [11]). However, the validation data set includes 21 onshore soils, 5 offshore soils and 21 soils used by Sreedeep et al. [18] and Abu-Hassanein [11].

It has been shown that a network with one hidden layer can approximate any continuous function, provided that sufficient connection weights are used [57]. To be in line with this assumption, one hidden layer was used. Choosing an appropriate number of neurons in the hidden layers is extremely important aspect in the back-propagation networks. Using too many neurons will increase the training time and may cause the over fitting problem (memorizing the training pattern rather than generalizing the prediction). On the other hand, using fewer hidden neurons often increases the likelihood of learning algorithm becoming trapped in a local

Table 6
The details of the optimal performance of the ANN-2 model.

ANN-2 model	Training function used	Epoch number	Performance indices				
			Data set	MAE (Ω m)	RMSE (Ω m)	VAF (%)	R^2
311	*Trainlm*	34	Training	18.78	37.90	67.24	0.674
			Validation	17.83	36.87	31.48	0.384
			Testing	15.16	26.34	59.36	0.656
	Trainscg	16	Training	19.83	38.69	65.86	0.660
			Validation	15.79	27.72	62.20	0.622
			Testing	14.40	21.21	74.41	0.744
321	*Trainlm*	14	Training	16.12	21.55	89.41	0.894
			Validation	14.14	19.50	81.35	0.820
			Testing	12.27	17.03	83.70	0.840
	Trainscg	34	Training	15.23	26.18	84.68	0.847
			Validation	13.30	22.66	74.28	0.746
			Testing	10.16	14.66	87.80	0.883
331	*Trainlm*	44	Training	12.76	17.96	92.64	0.926
			Validation	11.53	18.86	82.39	0.825
			Testing	10.88	14.96	87.08	0.876
	Trainscg	33	Training	14.47	26.84	84.58	0.838
			Validation	12.53	24.15	70.52	0.748
			Testing	8.67	14.30	87.76	0.918
341	*Trainlm*	78	Training	7.97	11.39	97.05	0.971
			Validation	8.66	12.54	92.44	0.925
			Testing	8.85	12.39	91.04	0.928
	Trainscg	47	Training	16.14	26.25	84.48	0.845
			Validation	12.81	21.73	77.16	0.804
			Testing	9.64	15.14	87.02	0.895
351	*Trainlm*	30	Training	6.70	9.12	98.10	0.981
			Validation	7.76	10.42	95.10	0.958
			Testing	6.55	10.14	94.43	0.956
	Trainscg	53	Training	13.73	24.11	87.14	0.873
			Validation	11.45	21.69	76.21	0.777
			Testing	8.62	13.49	89.57	0.942
361	*Trainlm*	47	Training	6.81	9.92	97.77	0.978
			Validation	5.50	7.94	96.81	0.969
			Testing	5.13	7.52	96.64	0.967
	Trainscg	30	Training	13.31	21.16	89.79	0.904
			Validation	10.68	17.57	84.38	0.844
			Testing	8.29	14.49	87.31	0.874
371	*Trainlm*	114	Training	**5.11**	**7.53**	**98.71**	**0.987**
			Validation	**6.09**	**8.40**	**96.87**	**0.971**
			Testing	**4.94**	**6.97**	**97.08**	**0.973**
	Trainscg	55	Training	11.72	18.22	92.43	0.930
			Validation	11.03	18.10	85.29	0.883
			Testing	8.41	13.25	91.23	0.949

minimum [58]. In this study, the optimum number of neurons in the hidden layer of both models was determined by varying their number starting with a minimum of 1 then increasing the network size up to $(2I+1)$, (I is the number of input parameters), in steps by adding 1 neuron each time. It should be noted that $(2I+1)$ is the upper limit for the number of hidden layer neurons needed to map any continuous function work with I inputs [59].

The neural network toolbox of MATLAB 7.0, a popular numerical computation and visualization software [21], was used for training and testing of MLPs. The Levenberg-Marquardt (*trainlm*) [50] and the Scaled Conjugate (*trainscg*) [51] training functions were used in the training stage. The gradient descent with momentum weight/bias learning function (*learngdm*) was used for adaption of the learning function. Different transfer functions (such as log-sigmoid

Table 7
Connection weights and biases of the best ANN models selected.

Model	Hidden neuron	Weight				Bias	
		Input neurons		Output neuron			
		S_r(%)	F (%)	R_T(°C-m/Watt)	R_E(Ω m)	Hidden layer	Output layer
ANN-1	1	–	22.66	24.24	1.84	−13.00	5.98
	2	–	−50.02	−51.74	−29.70	53.80	
	3	–	−15.52	10.07	16.63	0.38	
	4	–	22.47	−12.00	14.15	−1.20	
	5	–	8.44	−8.58	5.37	8.37	
ANN-2	1	−0.07	0.27	−6.31	−24.78	−0.13	−6.52
	2	−2.51	−15.00	−4.35	−16.16	7.07	
	3	6.24	−0.12	10.56	5.30	−4.74	
	4	−2.08	1.39	−8.67	19.96	1.32	
	5	−1.52	−14.89	−0.98	16.94	5.97	
	6	−49.24	11.20	3.53	20.34	−12.32	
	7	−4.75	2.50	6.62	0.73	−13.96	

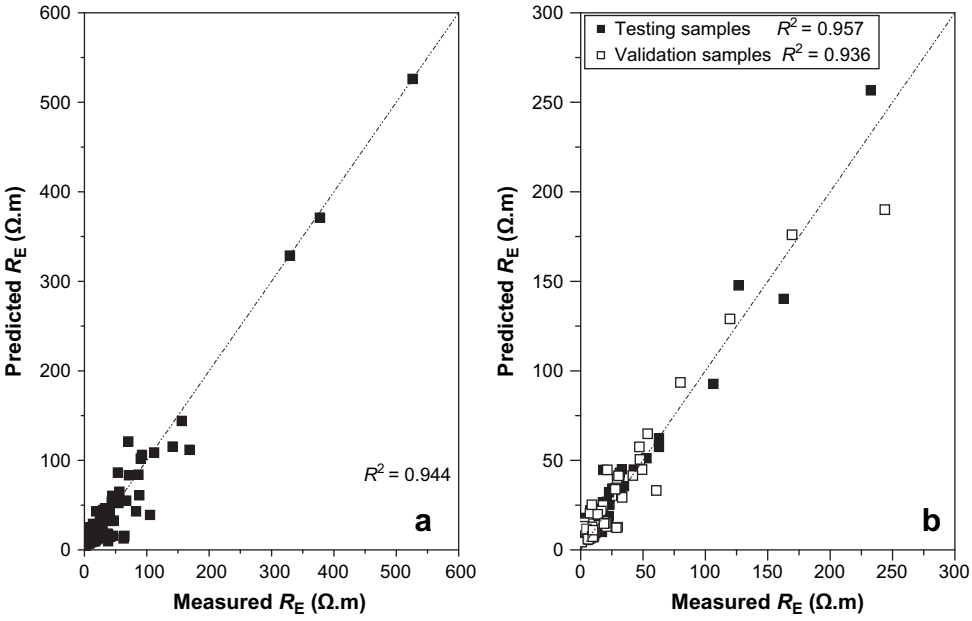

Fig. 2. Comparison of the measured/predicted R_E values from the model ANN-1 for a) training samples, and b) testing and validation samples.

[60] and tan-sigmoid [36]) were investigated to achieve the best performance in training as well as in testing. While using *trainlm*, two momentum factors, μ,(=0.01 and 0.001) were selected for the training process to search for the most efficient ANN architecture. The root mean square error RMSE was used to evaluate the performance of the developed ANN models. The performance of the network was examined for each network size until no significant improvement occurred.

5. Multiple regression analysis models for the prediction of R_E

Multiple regression analysis (MRA) was performed to predict R_E from its R_T and its saturation state (S_r). To achieve this, two MRA models (MRA-1 and MRA-2) were developed by using SPSS 8.0.0. The experimental data for the onshore and offshore samples (refer Tables 1 and 2) and the data reported by Sreedeep et al. [18] and Abu-Hassanein [11], for different types of soils (Table 3), were used in the development of these models. F and R_T were included in the model MRA-1, which yields Eq. (8). However, when F, S_r and R_T values were included in the model MRA-2, Eq. (9) was obtained.

$$R_E = -36.359 + 1.194F + 7.28\,R_T \quad R^2 = 0.454 \tag{8}$$

$$R_E = 8.413 + 1.105F - 0.387S_r + 6.97R_T \quad R^2 = 0.481 \tag{9}$$

6. Results and discussion

In this study, apart from RMSE, the performance indices (i.e., variance account for, VAF, which is represented by Eq. (10), mean absolute error, MAE, determination coefficient, R^2) were also computed to assess the performance of the developed models [29,61–64]. In Eq. (10), *var* denotes the variance, y is the measured

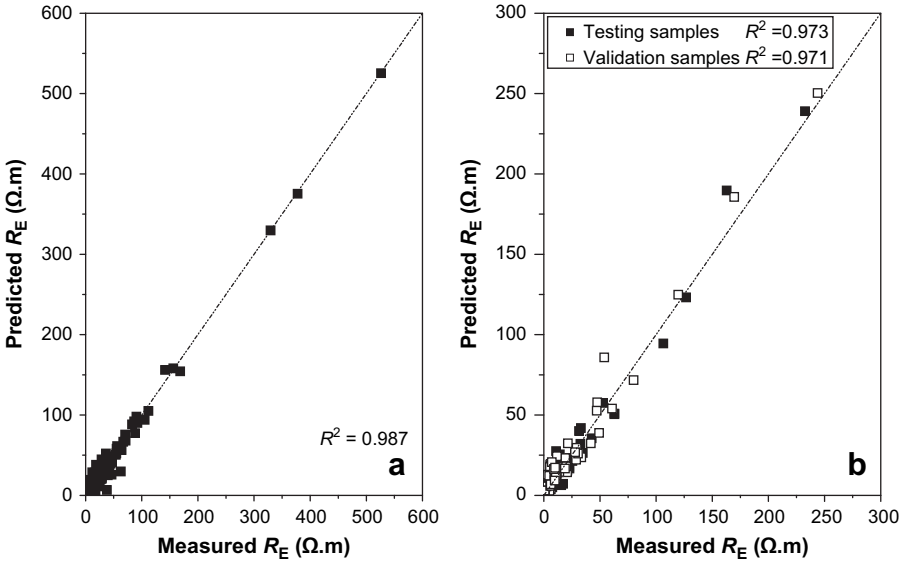

Fig. 3. Comparison of the measured/predicted R_E values from the model ANN-2 for a) training samples, and b) testing and validation samples.

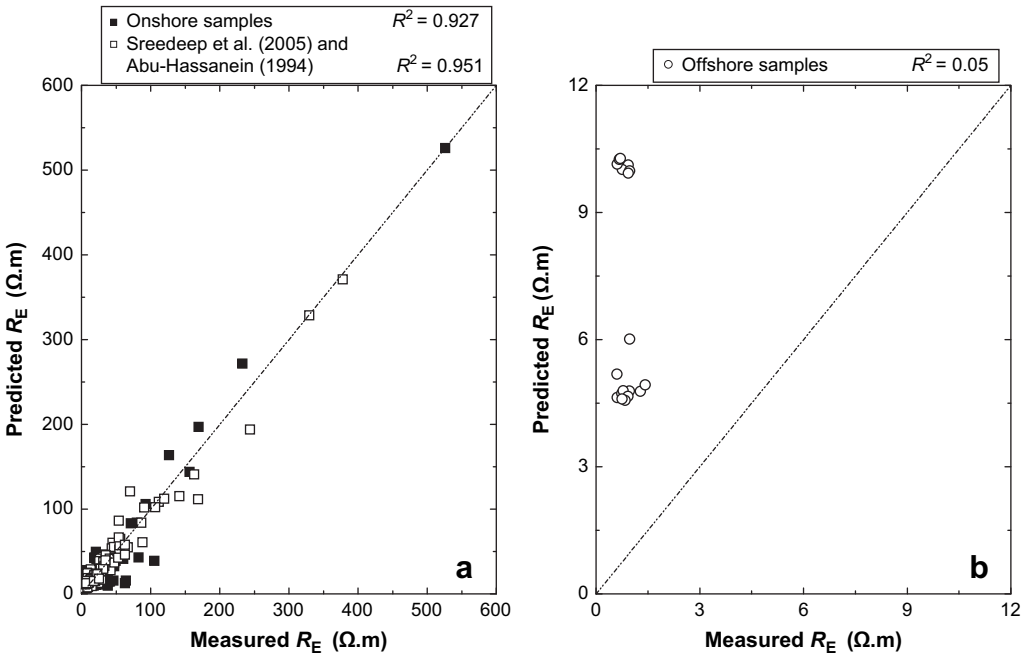

Fig. 4. a) Comparison of the measured/predicted R_E values from the model ANN-1 for onshore samples and the soils used by Sreedeep et al. [18] and Abu-Hassanein [11], and b) offshore samples.

value, and $\hat{y}$ is the predicted value. If VAF is 100%, the model is treated as excellent.

$$\mathrm{VAF} = \left[1 - \frac{\mathrm{var}\left(y - \hat{y}\right)}{\mathrm{var}(y)}\right] \times 100 \tag{10}$$

Details of the optimal performance of the ANN-1 and ANN-2 models are presented in Tables 5 and 6, respectively. Tables 5 and 6 show that the optimal performance of testing data set for ANN-1 and ANN-2 models are better than the training data set. This is possibly due to the cross validation technique [56] used as the stopping criterion to overcome over fitting. As mentioned earlier, in this technique, the training is stopped when the error on the validation set begins to increase and then testing data is fed into the networks to evaluate their performance. Later, performance of the network for training and testing processes was examined for each network size until no significant improvement occurred. Results presented in Tables 5 and 6 indicate that the cross validation technique [56] works quite well.

As mentioned earlier, a network with one hidden layer can approximate any continuous function, provided that sufficient connection weights are used [57]. Hence, to be in line with this assumption, one hidden layer was used in this study. It can be noted from Tables 5 and 6 that ANNs with one hidden layer and adequate number of hidden neurons are found to be quite useful as observed by earlier researchers [29,46,47].

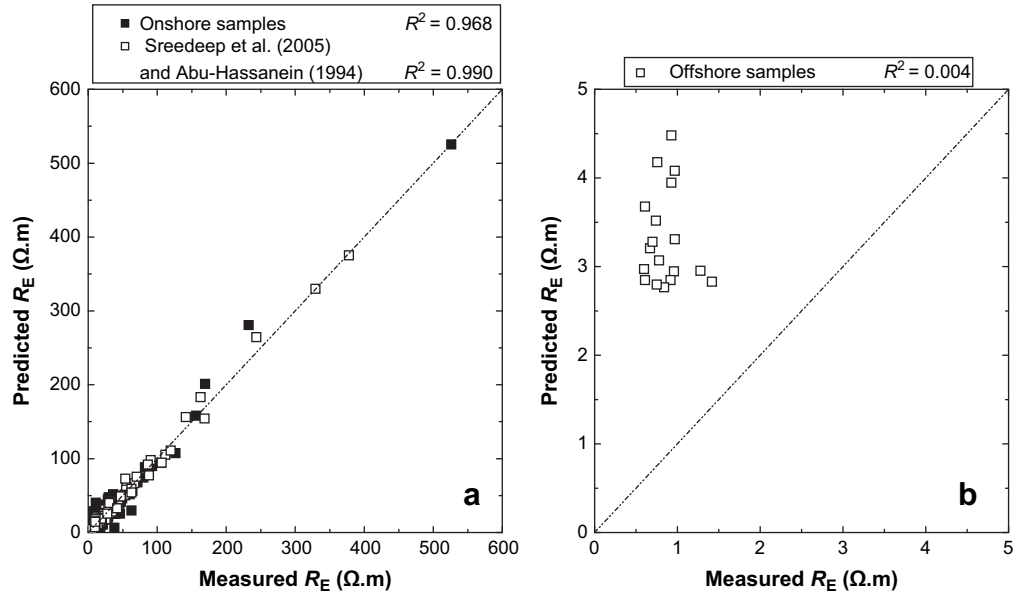

Fig. 5. Comparison of the measured/predicted R_E values from the model ANN-2 for a) onshore samples and the soils used by Sreedeep et al. [18] and Abu-Hassanein [11] , and b) offshore samples.

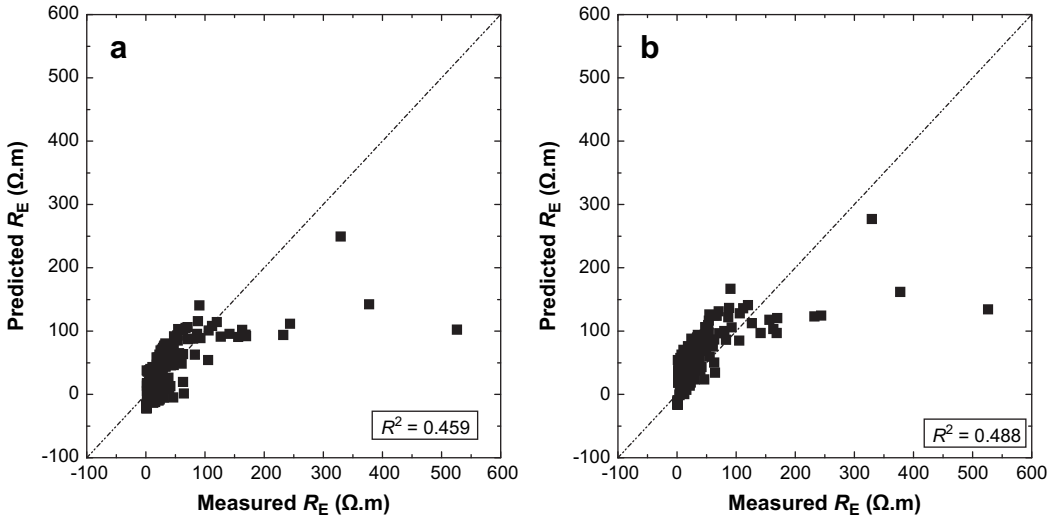

Fig. 6. Comparison of the measured/predicted R_E values from a) MRA-1, and b) MRA-2 for all samples.

Table 5 shows that ANN-1 with 5 hidden neurons using *trainlm* training function resulted in the minimum RMSE value of 9.15 Ω m in the testing phase. Therefore, it was chosen as the best ANN-1 model. Table 6 shows that ANN-2 with 7 hidden neurons using *trainlm* training function yields the minimum RMSE values of 7.53 Ω m and 6.97 Ω m in the training and testing phases, respectively. Therefore, it was chosen as the best ANN-2 model. Connection weights and biases for both optimal ANN models are presented in Table 7.

When compared the performance of the ANN-1 model (bold values in Table 5) with the ANN-2 model (bold values in Table 6), the ANN-2 model is able to predict electrical resistivity of different types of soils much more efficiently. This is mainly due to the fact that the ANN-2 model includes both the influences of physical composition and saturation.

A comparison of the experimental results vis-à-vis those obtained from both ANN models, for training, validation, and testing samples, is depicted in Figs. 2 and 3. It can be noted from Fig. 2 that R_E values obtained from ANN-1 model are quite close to the experimentally obtained R_E values. This shows that the ANN models are able to predict electrical resistivity of different types of soils quite efficiently, if their thermal resistivity and physical composition are known. However, ANN-2 model (Fig. 3) is found to yield better predictions than ANN-1 model (Fig. 2), as the R^2 value is much close to unity. As mentioned earlier, this is mainly due to the fact that the ANN-2 model includes both the influences of physical composition and saturation.

In addition, the measured R_E values were compared vis-à-vis with those obtained from both ANN models based on the soil types. To achieve this, samples used were categorized into two groups such as (a) onshore soils and the soils used by Sreedeep et al. [18] and Abu-Hassanein [11], and (b) offshore soils. The comparison of measured versus predicted R_E values from ANN-1 model is depicted in Fig. 4 for the first and second group samples, respectively. Similarly, the comparison of measured versus predicted R_E values from ANN-2 model is depicted in Fig. 5 for the first and second

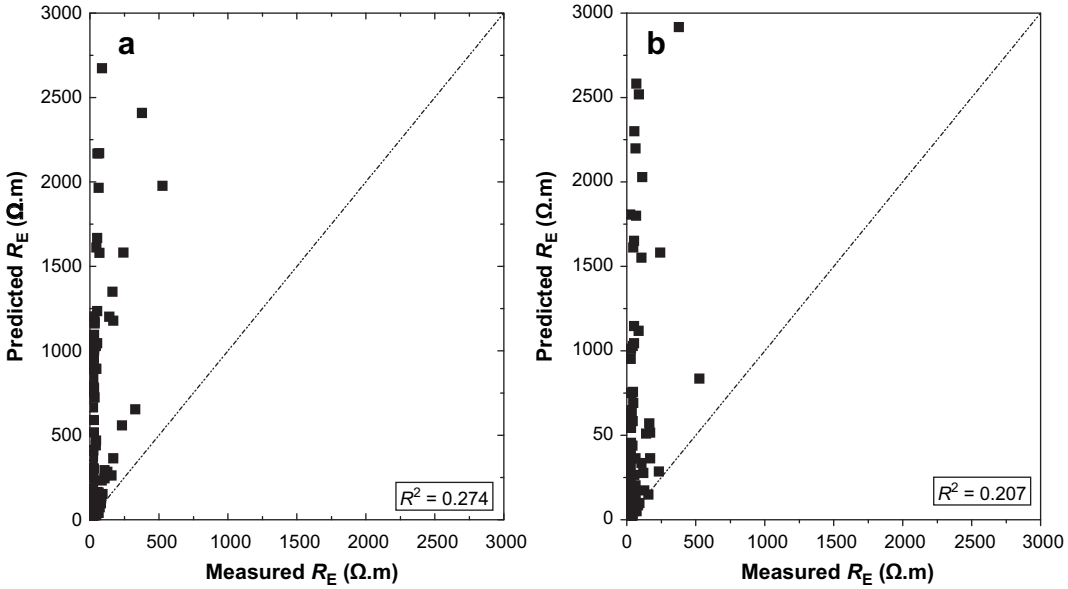

Fig. 7. Comparison of the measured/predicted R_E values from a) Eq. (2), and b) Eq. (3) for all samples.

Table 8
Performance indices for ANN, MRA and generalized models.

Model	Data	R^2	RMSE (Ω m)	MAE (Ω m)	VAF (%)
ANN-1	Training set	0.944	15.67	10.68	94.41
	Validation set	0.936	11.93	8.08	93.04
	Testing set	0.957	9.15	6.67	95.54
ANN-2	Training set	0.987	7.53	5.11	98.71
	Validation set	0.971	8.40	6.09	96.87
	Testing set	0.973	6.97	4.94	97.08
MRA-1	All set	0.459	41.99	22.67	45.91
MRA-2	All set	0.488	44.19	30.31	48.81

group samples, respectively. Figs. 4 and 5 show that both ANN models yield good predictions for onshore samples and the soils used by Sreedeep et al. [18] and Abu-Hassanein [11]. However, both ANN models yield poor predictions for offshore soils. This may be attributed to the fact that less data, only 18 data sets for offshore soils, were used in the development of both ANN models. It must also be appreciated that (refer Tables 1 and 2) R_E values for offshore samples is much lower, due to their high chloride content (>500 ppm). In general, for these samples, C_R reported by Eq. (3) should be multiplied by a factor 0.7.

To assess the performance of MRA models (Eqs. (8) and (9)), R_E was computed for different soil samples used in the ANN models. The computed R_E values from Eqs. (8) and (9) were compared with the values obtained experimentally, as shown in Fig. 6 for all samples, respectively. Fig. 6 shows that Eqs. (8) and (9) yield poor predictions.

To observe the performance of the generalized relationships Eqs. (2) and (3), R_E was computed for different soil samples used in the ANN models. The computed R_E values from Eqs. (2) and (3) were compared with the values obtained experimentally, as shown in Fig. 7 for all samples. Fig. 7 shows that Eqs. (2) and (3) yield very poor predictions. This is possibly due to the fact that Eqs. (2) and (3) were derived by using the experimental data different from the data used in this study.

Values of R^2, RMSE, MAE, and VAF for the optimal ANN and MRA models are listed in Table 8, which exhibits that both ANN models are efficient in predicting the soil electrical resistivity while MRA model yield poor predictions.

7. Conclusions

In this study, two different ANN models (ANN-1 and ANN-2) and MRA models (MRA-1 and MRA-2) have been developed for determining the electrical resistivity of soils just by knowing their thermal resistivity, soil type and the degree of saturation. For this purpose, the experimental data for the onshore and offshore samples and the data reported in the literature for different types of soils were used. While, models ANN-1 and MRA-1 have two input parameters, F and R_T, models ANN-2 and MRA-2 have three input parameters, S_r, F and R_T. Both the Levenberg-Marquardt and the Scaled Conjugate learning algorithms were used in the training stage of the ANN models. One hidden layer is found to be sufficient for these ANN models. The results obtained from ANN and MRA models were compared vis-à-vis those obtained from the experiments. It is found that the values predicted from the ANN models match with the experimental values much better than those obtained from MRA models. Further, ANN-2 model is found to yield better predictions than the ANN-1 model. In addition, the performance indices such as coefficient of determination, root mean square error, mean absolute error, and variance were used to assess the performance of the models developed. The study demonstrates that the ANN models are able to predict electrical resistivity of different soils, quite efficiently, and are superior to the MRA models. Thus, ANN models can be used to predict electrical resistivity of soils as an inexpensive substitute for the laboratory testing, quite easily and efficiently.

References

[1] R.J. Kalinski, W.E. Kelly, Estimating water content of soils from electrical resistivity, Geotechnical Testing Journal 16 (3) (1993) 323–329.
[2] W. McCarter, The electrical resistivity characteristics of compacted clays, Geotechnique 34 (2) (1984) 263–267.
[3] O. Mazac, M. Cislerove, W.E. Kelly, I. Landa, D. Venhodova, Determination of hydraulic conductivities by surface geoelectrical methods, in: S. Ward, (Ed.), Geotechnical and Environmental Geophysics, Vol II, Soc. Explor. Geophys. (1990) 125–131.
[4] A.E. Ronald, C.G. Ronald, Electrical resistivity used to measure liquefaction of sand, Journal of Geotechnical Engineering 108 (GT5) (1982) 779–783.
[5] D.W. Schultz, B.M. Duff, W.R. Peters, Performance of an Electrical Resistivity Technique for Detecting and Locating Geomembrane Failures, International Conference on Geomembranes, Denver, USA, (1984) 445–449.
[6] B. McCollum, K.H. Logan, Electrolytic corrosion of Iron in soils, Bureau of Standards, Technologic Paper 24 (1930).
[7] G.F. Tagg, Earth Resistances, Newnes, London, 1964.
[8] R. Butterfield, I.W. Jhonston, The influence of electro-osmosis on metallic piles in clay, Geotechnique 30 (1) (1980) 17–38.
[9] B.W. Gunnink, J. El-Jayyousi, Soil-fabric measurement using conduction phase porosimetry, Journal of Geotechnical Engineering Division 119 (6) (1993) 1019–1035.
[10] P.F. Shea, J.N. Luthin, An investigation of the use of the four electrode probe for measuring soil salinity in situ, Soil Science 92 (1961) 331–339.
[11] Z.S. Abu-Hassanein, Use of electrical resistivity measurement as a quality control tool for compacted clay liners, M.S. Thesis, University of Wisconsin, Madison (1994).
[12] H.R. Thomas, Modeling two-dimensional heat and moisture transfer in soils including gravity effects, International Journal of Numerical and Analytical Methods in Geomechanics 9 (1985) 573–578.
[13] D.N. Singh, M.V.B.B.G. Rao, Laboratory measurement of soil thermal resistivity, Geotechnical Engineering Bulletin 7 (3) (1998) 179–199.
[14] M.V.B.B.G. Rao, D.N. Singh, A generalized relationship to estimate thermal resistivity of soils, Canadian Geotechnical Journal 36 (4) (1999) 767–773.
[15] D.N. Singh, K. Devid, Generalized relationships for estimating soil thermal resistivity, Experimental. Thermal and Fluid Science 22 (2000) 133–143.
[16] P.K. Kolay, D.N. Singh, Application of coal ash in fluid thermal beds, Journal of Materials Civil Engineering 14 (5) (2002) 441–444.
[17] D.N. Singh, S.J. Kuriyan, K.C. Manthena, A generalized relationships between soil electrical and thermal resistivities, Experimental Thermal and Fluid Science 25 (2001) 175–181.
[18] S. Sreedeep, A.C. Reshma, D.N. Singh, Generalized relationship for determining soil electrical resistivity from its thermal resistivity, Experimental Thermal and Fluid Science 29 (2005) 217–226.
[19] D.G. Toll, Artificial intelligence applications in geotechnical engineering, Electronic Journal of Geotechnical Engineering 1 (1996).
[20] M.A. Shahin, M.B. Jaksa, H.R. Maier, Artificial neural network applications in geotechnical engineering, Australian Geomechanics 36 (1) (2001) 49–62.
[21] M. Banimahd, S.S. Yasrobi, P. Woodward, Artificial neural network for stress-strain behavior of sandy soils: knowledge based verification, Computers and Geotechnics 32 (2005) 377–386.
[22] N. Caglar, H. Arman, The applicability of neural networks in the determination of soil properties, Bulletin of Engineering Geology and the Environment 66 (2007) 295–301.
[23] Y.S. Kim, B.T. Kim, Use of artificial neural networks in the prediction of liquefaction resistance of sands, Journal of Geotechnical and Geo-environmental Engineering 132 (11) (2006) 1502–1504.
[24] P.U. Kurup, E.P. Griffin, Prediction of soil composition from CPT data using general regression neural network, Journal of Computing in Civil Engineering 20 (4) (2006) 281–289.
[25] S.K. Sinha, M.C. Wang, Artificial neural network prediction models for soil compaction and permeability, Geotechnical and Geological Engineering (August 17, 2007).
[26] I.M. Lee, J.H. Lee, Prediction of pile bearing capacity using artificial neural networks, Computers and Geotechnics 18 (3) (1996) 189–200.
[27] C.I. Teh, K.S. Wong, A.T.C. Goh, S. Jaritngam, Prediction of pile capacity using neural networks, Journal of Computing in Civil Engineering 11 (2) (1997) 129–138.
[28] M.A. Shahin, H.R. Maier, M.B. Jaksa, Predicting settlement of shallow foundations using neural networks, Journal of Geotechnical and Geoenvironmental Engineering 128 (9) (2002) 785–793.
[29] Y. Erzin, B.H. Rao, D.N. Singh, Artificial neural networks for predicting soil thermal resistivity, International Journal of Thermal Science 47 (10) (2008) 1347–1358.
[30] G.W. Ellis, C. Yao, R. Zhao, D. Penumadu, Stress-strain modeling of sands using artificial neural networks, Journal of Geotechnical Engineering 121 (5) (1995) 429–435.
[31] P. Gandhidasan, M.A. Mohandes, Predictions of vapor pressures of aqueous desiccants for cooling applications by using artificial neural networks, Applied Thermal Engineering 28 (2008) 126–135.

[32] R. Hecht-Nielsen, Neurocomputing, Addison-Wesley, Boston, 1990.
[33] J.M. Zurada, Introduction to Artificial Neural Systems, West, St. Paul, Minn, 1992.
[34] L.V. Fausett, Fundamentals of Neural Networks: Architecture, Algorithms and Applications, Prentice-Hall, Englewood Cliffs, N.J, 1994.
[35] B.D. Ripley, Pattern Recognition and Neural Networks, Cambridge University Press, Cambridge, 1996.
[36] P. Orbanić, M. Fajdiga, A neural network approach to describing the fretting fatigue in aluminum-steel couplings, International Journal of Fatigue 25 (2003) 201–207.
[37] H. Sonmez, C. Gokceoglu, H.A. Nefeslioglu, A. Kayabasi, Estimation of rock modulus: for intact rocks with an artificial neural network and for rock masses with a new empirical equation, International Journal of Rock Mechanical and Mining Sciences 43 (2) (2005) 224–235.
[38] I. Kaastra, M. Boyd, Designing a neural network for forecasting financial and economic time series, Neurocomputing 10 (3) (1996) 215–236.
[39] Kanellopoulas, G.G. Wilkinson, Strategies and best practice for neural network image classification, International Journal of Remote Sensing 18 (1997) 711–725.
[40] M.A. Grima, R. Babuska, Fuzzy model for the prediction of unconfined compressive strength of rock samples, International Journal of Rock Mechanical and Mining Science 36 (1999) 339–349.
[41] M.E. Haque, K.V. Sudhakar, ANN back-propagation prediction model for fracture toughness in microalloy steel, International Journal of Fatigue 24 (2002) 1003–1010.
[42] Y.M. Najjar, I.A. Basheer, W.A. Naouss, Neural modeling of Kansas soil swelling, Transportation Research Record 1526 (1996) 14–19.
[43] H. Kim, A.F. Rauch, C.T. Haas, Automated quality assessment of stone aggregates based on laser imaging and a neural network, Journal of Computing in Civil Engineering 18 (1) (2004) 58–64.
[44] A.T.C. Goh, Back-propagation neural networks for modeling complex systems, Artificial Intelligence in Engineering 9 (1995a) 143–151.
[45] A.T.C. Goh, Modeling soil correlations using neural networks, Journal of Computing in Civil Engineering 9 (4) (1995b) 275–278.
[46] F. Amegashie, J.Q. Shang, E. Yanful, W. Ding, S. Al-Martini, Using complex permittivity and artificial neural networks to identify and classify copper, zinc, and lead contamination in soil, Canadian Geotechnical Journal 43 (2006) 100–109.
[47] J.J. Shi, Reduction prediction error by transforming input data for neural networks, Journal of Computing in Civil Engineering 18 (2) (2000) 105–114.
[48] M.A. Shahin, H.R. Maier, M.B. Jaksa, Data division for developing neural networks applied to geotechnical engineering, Journal of Computing in Civil Engineering 18 (2) (2004) 105–114.
[49] M.A. Shahin, M.B. Jaksa, Neural network prediction of pullout capacity of marquee ground anchors, Computers and Geotechnics 32 (2005) 153–163.
[50] H. Demuth, M. Beale, M. Hagan, Neural Network Toolbox User's Guide, The Math Works, Inc., Natick, Mass, 2006.
[51] M.F. Moller, A scaled conjugate gradient algorithm for fast supervised learning, Neural Networks 6 (1993) 525–533.
[52] ASTM, D-422-63 Standard Test Method for Particle Size Analysis of Soils. Annual Book of ASTM Standards 04.08, ASTM International, West Conshohocken, USA, 1994, pp. 10–16.
[53] D. Astm, 5550, Standard test method for specific gravity of soil solids by gas pycnometer, Annual book of ASTM standards 04.08, ASTM, West Conshohocken, PA, USA, 2001, 1–4.
[54] A. Dalinaidu, D.N. Singh, A generalized procedure for determining thermal resistivity of soils, International Journal of Thermal Sciences 43 (1) (2004) 43–51.
[55] J.M. Twomey, A.E. Smith, Validation and verification, in: N. Kartam, I. Flood, J.H. Garrett (Eds.), Artificial Neural Networks for Civil Engineers: Fundamentals and Applications, ASCE, New York, 1997, pp. 44–64.
[56] M. Stone, Cross-validatory choice and assessment of statistical predictions, Journal of Royal Statistical Society B 36 (1974) 111–147.
[57] K. Hornik, M. Stinchcombe, H. White, Multilayer feed forward networks are universal approximators, Neural Networks 2 (1989) 359–366.
[58] N.O. Nawari, R. Liang, J. Nusariat, Artificial intelligence techniques for the design and analysis of deep foundations, Electronic Journal of Geotechnical Engineering (1999).http://geotech.civeng.okstate.edu/ejge/ppr9909/index.html.
[59] M. Caudill, Neural Networks Primer, Part III, Al Expert 3 (6) (1988) 59–61.
[60] M.G. Sakellariou, M.D. Ferentinou, A study of slope stability prediction using neural networks, Geotechnical and Geological Engineering 23 (2005) 419–445.
[61] J. Finol, Y.K. Guo, X.D. Jing, A rule based fuzzy model for the prediction of petrophysical rock parameters, Journal of Petroleum Science and Engineering 29 (2001) 97–113.
[62] C. Gokceoglu, A fuzzy triangular chart to predict the uniaxial compressive strength of Ankara agglomerates from their petrographic composition, Engineering Geology 66 (2002) 39–51.
[63] Y. Erzin, Artificial neural networks approach for swell pressure versus soil suction behavior, Canadian Geotechnical Journal 44 (2007) 1215–1223.
[64] Y. Yukselen, Y. Erzin, Artificial neural networks approach for zeta potential of montmorillonite in the presence of different cations, Environmental Geology 54 (2008) 1059–1066.